ASSESSING THE EFFECT OF OBESITY BY OPTICAL SPECTROSCOPY

An Undergraduate Research Scholars Thesis

by

CASSIDY GOBBELL

Submitted to the Undergraduate Research Scholars program
Texas A&M University
in partial fulfillment of the requirements for the designation as an

UNDERGRADUATE RESEARCH SCHOLAR

Approved by
Research Advisor: Dr. Vladislav Yakovlev

May 2016

Major: Biomedical Engineering

TABLE OF CONTENTS

ABSTRACT

Assessing the Effect of Obesity by Optical Spectroscopy

Cassidy Gobbell
Department of Biomedical Engineering
Texas A&M University

Research Advisor: Dr. Vladislav Yakovlev
Department of Biomedical Engineering

It is hypothesized that an increase in adipose tissue rigidity can both limit swelling and shrinking of adipocytes which predisposes people to obesity related health problems. Taking into account the alarming trend of increased obesity rates in the nation, it is important to examine the effect of diet on the body. Raman spectroscopy allows non-invasive chemical assessment, while Brillouin spectroscopy affords non-invasive measurements of local elasticity of tissues, which, as we hypothesize, are being affected by obesity. In this study, a group of rats were fed a diet supplemented with high-lipids while the control group was fed a regular diet. Two spectroscopic techniques were used to evaluate the variations of chemical and mechanical properties in the skin, inguinal and interscapular adipose tissues between the two groups. Supplementary measurements were collected from the femoral vein and artery.

CHAPTER I

INTRODUCTION

Adipose tissue and obesity

Adipose tissue is a loose connective tissue composed of adipocytes, fibroblasts, and immune cells. These cells dwell in a collagenous extracellular matrix with a network of blood vessels [1]. Figure 1 gives a depiction of the fibrous connective tissue that adipocytes dwell. Adipose tissue provides thermal insulation and mechanical protection, and additionally, is an endocrine organ with a role in metabolic regulation and physiological homeostasis [2].

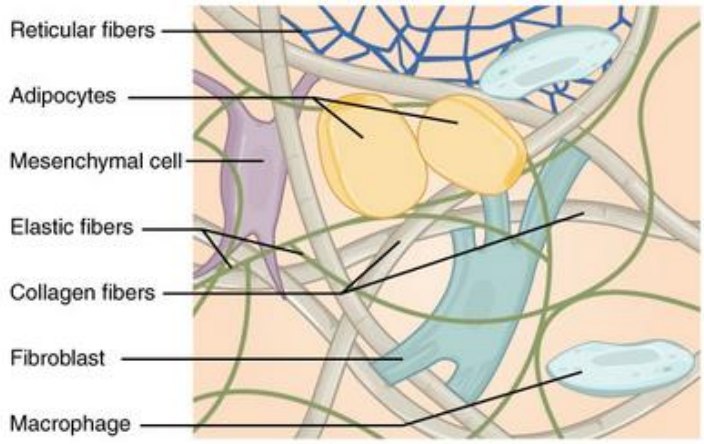

Figure 1. Fibrous Connective Tissue. Contains collagen, elastic, and reticular fibers, adipocytes, fibroblasts, and immune cells such as macrophages [3].

White adipose tissue is the principal form of adipose tissue. Its major role is the storage of surplus dietary triglycerides and it expands with obesity [2]. Conversely, brown adipose tissue's function is to transfer energy from food into heat [4]. Obesity is a low-grade inflammatory disease characterized by an increase inflammatory proteins in obese subjects [5]–[7].

Obesity's effect on adipose tissue

Typically adipose tissue has a high expandability, but as a result of lipid uptake, adipocytes become hypertrophic and the number of immune cells increase [7], [8]. Because of this, the extracellular matrix changes through an increase in the deposition of collagen and the adipose tissue becomes more rigid [9]. The adipose tissue can also become fibrotic. It is hypothesized that this fibrosis limits the ability of the adipocytes to swell when additional storage is needed or to shrink during weight loss [10]–[13]. These limits on the adipocytes predisposes an individual to obesity related health problems such as cardiovascular disease and diabetes [5], [11], [14]–[17]. Therefore, it is important to better understand the changing mechanical properties of adipose tissue. There are only few studies on the mechanical properties of adipose tissue relating to the function of fat storage [18], [19]. With the combined use of Brillouin and Raman spectroscopy, we can better understand the changing longitudinal modulus of adipose tissue in obese subjects.

Raman and Brillouin spectroscopy

Brillouin spectroscopy is an emerging tool that has been used to provide information on the samples' viscoelastic properties [20], is used in remote sensing [21], [22], material science [23], [24], and biomedical applications [25]–[30]. Raman spectroscopy has been used in the medical industry for diagnostic sensing including non-invasive deep tissue diagnosis [31]. Since both are optical techniques, measuring Brillouin and Raman spectra simultaneously can offer complementary information about a material's chemical and mechanical structure [26].

Spontaneous Brillouin Scattering

Both Raman and Brillouin spectroscopy result from inelastic scattering of light. This scattering causes a shift in the frequency of light due to some resonant property [26]. Spontaneous Brillouin scattering is a process of the inelastic interaction between the incident electromagnetic wave and the acoustic phonons in the medium of the material under study [32]. The incident electromagnetic wave experiences a frequency shift proportional to the speed of sound in the medium [32]. As a result, the medium's elastic modulus, which is directly related to the speed of sound in the medium, can be determined by measuring the Brillouin frequency shift [32]. The magnitude of the Brillouin frequency shift (Ω) can be determined using equation (1)

$$\Omega = 2\left(\frac{nV_L}{\lambda_o}\right)\sin\left(\frac{\theta}{2}\right) \quad (1)$$

where n is the index of refraction of the material, V_L is the speed of sound of the material, λ_o is the wavelength of incident light, and θ is the angle between incident and scattered light. If Ω is known, V_L can be calculated using equation (1). After V_L is found, equation (2) can be used to find the longitudinal modulus, M, where ρ is the density of the material [23].

$$V_L = (M/\rho)^{1/2} \quad (2)$$

Raman Spectroscopy

In Raman spectroscopy, the incident light interacts with the molecular vibrations of the material which causes the frequency of light to shift. This Raman shift (ω_s) is determined according to

equation (3) where ω_o is the pump laser frequency, and Ω is the energy difference between the excited vibrational level and the ground state [26].

$$\omega_s = \omega_o \pm \Omega \quad (3)$$

Consequently, Raman spectroscopy can give specific vibrational signatures of chemical bonds [33]. Finally, measuring the elastic moduli of adipose tissues using Brillouin spectroscopy in conjunction with Raman spectroscopy can be an effective, non-invasive, and label-free tool in determining if and how diet affects these tissue samples.

CHAPTER II

EXPERIMENTAL APPROACH

Experimental setup

A diagram of the experimental setup is displayed in Figure 2. The setup is an optimized background-free Brillouin spectrometer based on an atomic molecular absorption filter [32], [34]. The source of incident radiation was a 532 nm single-frequency laser (Lasermate Inc.; GMSL-532-100FHA). The center wavelength was specified at 534.3157 nm ± 3 pm, the maximum power was about 100 mW, and the nominal output linewidth was about 640 kHz. The spot size was about 1.5 microns in diameter, and its penetration depth was manually tuned to be about 100 microns. In order to prevent unwanted feedback from the setup, an optical isolator (Electro-Optics Technology, Inc.; BB-8-05-I090) was employed. In addition, a polarizing beam splitter was positioned in the beam path in order to direct the backscattered light towards the confocal pinhole. A microscope objective lens (Nikon Inc., CFI Plan Fluor 20x, N.A. = 0.5) focused the pump onto the sample and collected the back-scattered light. A Faraday optical rotator (Electro-Optics Technology, Inc.) was placed prior to the objective lens to serve the purpose of rotating the polarization of the back-reflected beam by 90°. The backscatter beam was split by a long-pass filter and sent to either a VIPA (Virtually Imaged Phase Array) spectrometer for Brillouin analysis or a Raman spectrometer. A VIPA is a fully parallel spectrometer that improves the detection efficiency nearly 100 times better than previous approaches [26] and can be used to acquire 2D *in situ* images of biological tissues [32], [34]. For more information on the VIPA see Scarcelli and Yun [26] or Meng [32], [34]. For all the measurements the power at the

sample was less than 40 mW, and no observable damage occurred during the course of experiments.

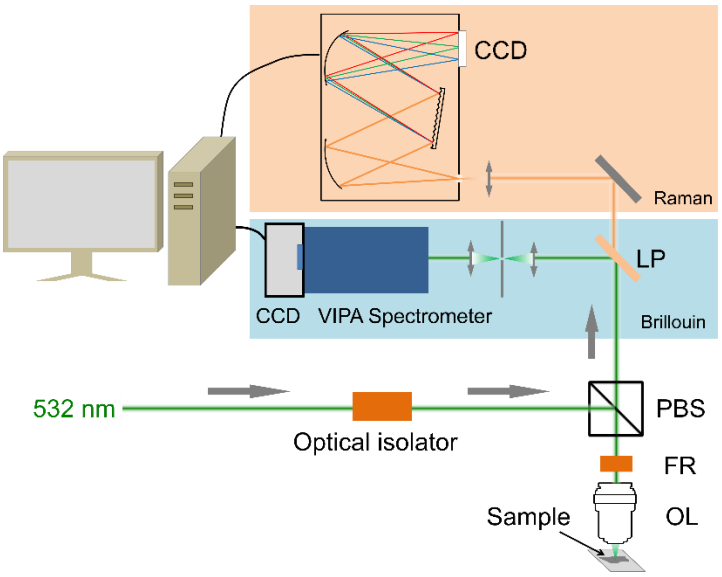

Figure 2. Diagram of the optical setup for both Brillouin and Raman spectroscopy. OL: microscope objective lens, FR: Faraday rotator, LP: long-pass filter, VIPA: virtually imaged phased array.

The diagram of the VIPA spectrometer is depicted in more detail in Figure 3. The input beam was coupled into a temperature-tunable iodine absorption cell (Opthos Instruments, Inc) which remained at 110 ± 2° F. In order to filter out the undesired molecular emission and remaining Raman signal, a 532 nm line filter was placed behind the iodine cell. The remainder of the VIPA spectrometer followed the design described by Scarcelli and Yun [26]. The VIPAs (Model: OP-5642, Light Machinery Inc.) were designed for 532-nm applications and had a nominal free spectral range (FSR) of 33.3 GHz. In order that the angular dispersion of the Brillouin component and the elastic component could be transferred into spatial dispersion, a spherical lens with a focal length of 1000 nm was positioned after the VIPA. Finally, a CCD camera

(Model: Newton 971, Andor Technology, Inc) was placed at the focal plane of the lens to obtain Brillouin spectra.

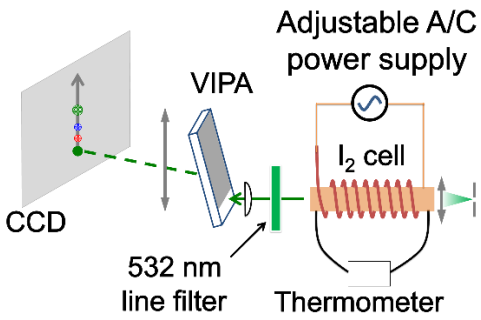

Figure 3. Detailed schematic of VIPA spectrometer.

Methodology

The samples for the current study were obtained from adult male Sprague-Dawley rats that were generously provided by Dr. A. Gashev (Texas A&M University, Department of Medical Physiology). All animal procedures for the study were reviewed and approved by Texas A&M's Institutional Animal Care and Use Committee. There were two groups of rats that were tested. The first group consisted of control rats (C), and the second group was fed a high lipid diet (L). Photos of respective rats that samples were taken from can be seen in Figure 4.

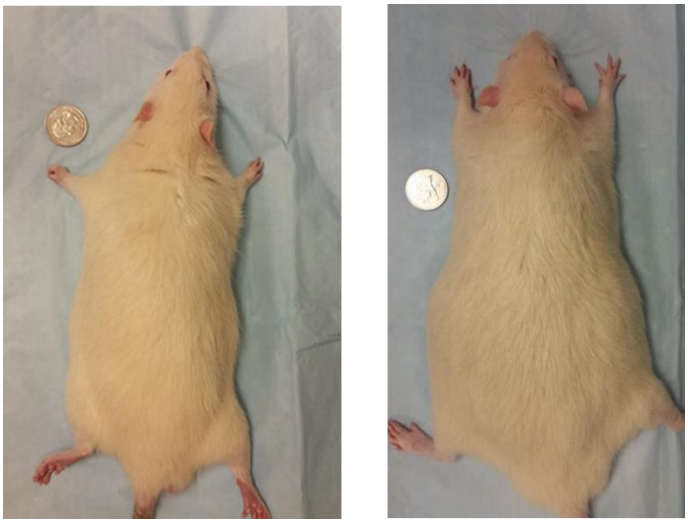

Figure 4. Representative photos of rats used in study. Left – Control rat; Right – High lipid diet rat

Samples from three to five rats from each group were taken and stored on ice. The samples seen in Figure 5 consisted of inguinal white adipose tissue (IWAT), interscapular brown adipose tissue (IBAT), abdominal skin, and the femoral vein and artery. Five to ten random data points from the IWAT, IBAT, and skin samples were taken. For the vessel, a line scan that moved across the vessel was used, and data points were taken every 50-100 μm. The scan began on the lipid-rich portion of the sample and scanned across the whole vessel and into another lipid-rich portion. See Figure 6 for a graphic displaying the line scan. Once the data was collected, it was analyzed using MATLAB software in order to find the Brillouin shift of each data point. The data points were also examined using a peak analysis of the Raman spectra that was acquired.

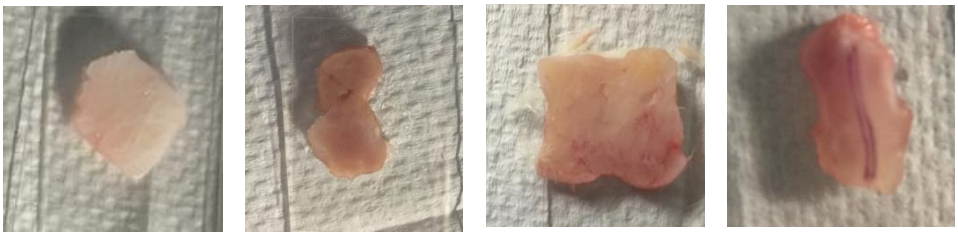

(a) (b) (c) (d)

Figure 5. Photographs of each type of sample. (a) inguinal white adipose tissue, (b) interscapular brown adipose tissue, (c) abdominal skin, and (d) femoral vein and artery.

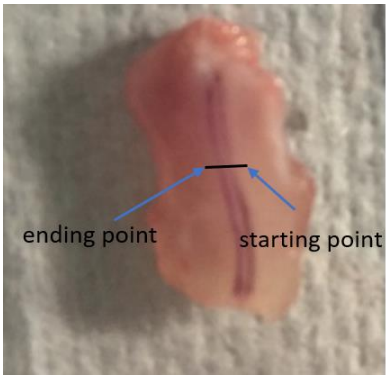

Figure 6. Starting and ending point of line scan. Data was acquired every 50 or 100 μm.

CHAPTER III

RESULTS

Representative Brillouin and Raman spectra

Representative Brillouin data for each sample (IWAT, IBAT, Skin, and Vessel) is shown in Appendix A as Figure A1. Due to a number of absorption lines contributed by the molecular iodine, Brillouin peaks are split into multiple peaks, and the physics of this phenomenon is illustrated in Figure 7. The data in Figure A1 depict the "Filtered Brillouin" spectra of each sample. Comparing the spectra in Figure A1, it can be seen that the IBAT samples had the best signal since the Stokes and Anti-Stokes peaks are prominent; however, the other samples generally had large enough anti-stokes peaks for the Brillouin frequency shift to be found.

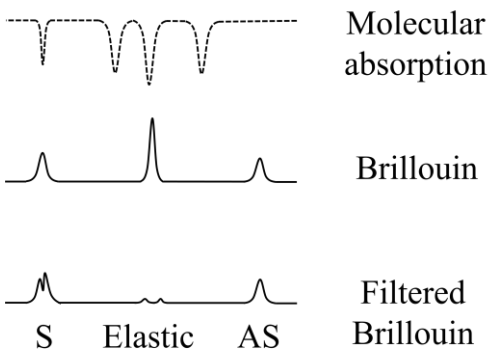

Figure 7. Origin of the absorption dips splitting the Brillouin peaks. S – Stokes, AS – Anti-Stokes.

Figure A2 displays representative Raman data for each sample. The data in the IBAT and IWAT samples was homogeneous, but this was not the case with the data gathered in the skin and vessel samples. As seen in Figure A2, there were two sharp peaks. One peak occurred at 2817-2849

cm^{-1} which represented CH_2 symmetric stretch of lipids characterizing a change in the amount of lipid [35]. The other peak occurred around 2900-2938 cm^{-1}. A peak in this range represents a CH stretch in lipids and proteins [35]. Once the Raman data was normalized, the location and peak heights were found for these two prominent peaks. The peak height in the lipid only range was divided by the peak height in the lipid and protein range in order to get a ratio of the lipid to protein content. A sample with a ratio that was lower than 0.75 was deemed "protein rich." The cut-off ratio 0.75 followed closely with a qualitative analysis that the Raman spectra resembled more of sharp peak rather than a plateau if the sample was "protein rich." When calculating and analyzing then Brillouin shifts, the spectra of the skin and vessel samples were separated using this qualitative and quantitative analysis.

Brillouin frequency shift analysis

For the Brillouin analysis, the locations of each elastic peak were found and associated with increasing frequencies with steps of 33.3 Hz (FSR). These new locations were plotted using a spline interpolation. The locations of the anti-stokes peaks were found and plotted on the new line. The distance from the anti-stokes peaks to the elastic peaks in the frequency domain was the Brillouin shift of that sample in GHz. The mean and standard error of the Brillouin shifts for each sample were calculated and are depicted in the graphs in Figure 8. Looking back at Equations 1 and 2 it can be noted that the Brillouin shift and longitudinal modulus are directly related. Knowing this, an increase in Brillouin shift can be associated with an increase in modulus if the density of the sample is known. The comparison in Figure 7 only uses the lipid-rich data collected from the skin and vessel samples.

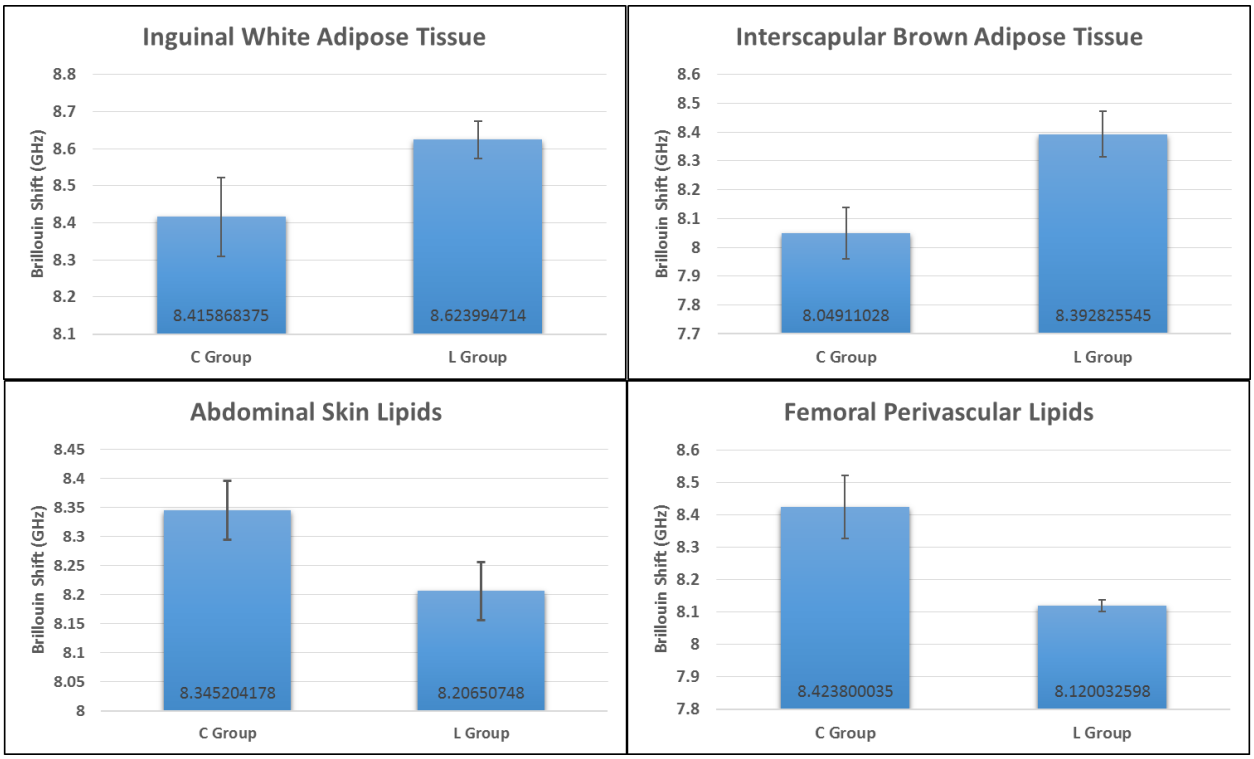

Figure 8. Comparing the means and standard errors of the Brillouin shifts of each sample. C: control group, L: high lipid diet group.

Looking at Figure 8, there is an obvious increase in the Brillouin shifts from the control group to the high-lipid diet group for the IWAT and IBAT samples. This could be due to the fact that the tissue around the brown and white adipose tissue is more rigid to begin with, so the adipocytes had less room to expand and thus had an increase in modulus. It is also important to note that the data for these samples were the most consistent. The Raman spectra for IWAT and IBAT was almost identical, and the Brillouin spectra was easier to analyze since these samples produced better signal. On the other hand, there was a decrease in the average Brillouin shift between the control and high-lipid groups when inspecting the skin and vessel data. Dissimilar to the white and brown fat, the tissue surrounding the abdominal and perivascular lipids is not as rigid, so the adipocytes did have more room to expand and did not become more rigid. Again, it is important to say that these two samples had worse signal and were categorized using a primarily qualitative

method. Keeping these things in mind, it can safely be said that there was in increase in longitudinal modulus between the control and high-lipid diet rats when analyzing purely adipose samples.

Line scan of control femoral vessel

The results of the line scan for the vessel can potentially give more data about the relationship between the Brillouin shifts and Raman data lipid to protein ratios. The representative data is shown below. The Brillouin shifts that were found for each acquisition taken every 50 μm are depicted in Figure 9, and the lipid to protein ratios found using the Raman data are in Table 1.

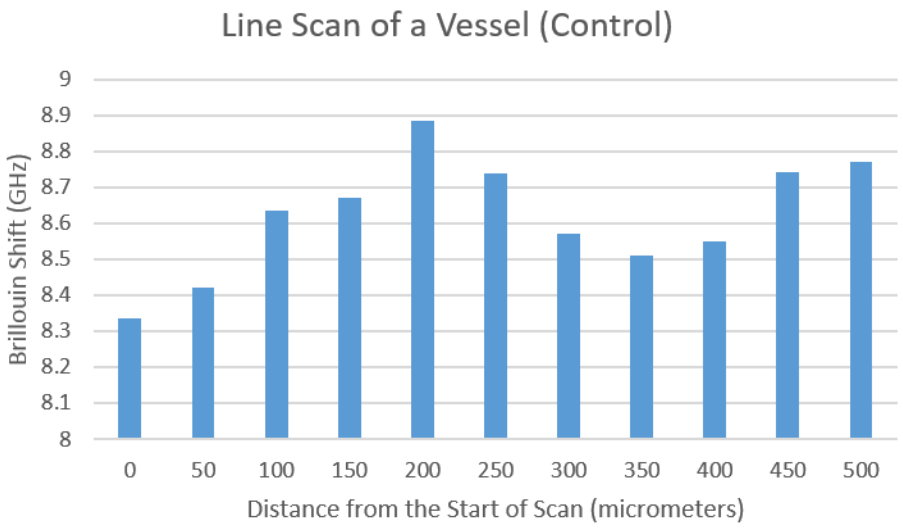

Figure 9. Brillouin Shifts using a line scan where each point was taken every 100 μm.

Table 1. Lipid to protein ratios gathered using the Raman spectra of a control vessel.

Distance from Start of Scan (μm)	Lipid Rich to Protein Rich Ratio
0	0.809
50	0.851
100	lipid rich peak not detected
150	0.667
200	0.660
250	0.694
300	0.806
350	0.816
400	0.942
450	1.03
500	0.989

Based solely on the data in Figure 10 and values in Table 1, there is not a significant trend between Brillouin shift and lipid to protein ratio except that acquisitions that had a ratio of ~0.80-0.85 had the lowest Brillouin shifts. This could indicate that samples with more of a mixture of protein and lipid had a lower elastic modulus than samples with mostly protein or mostly lipid. All in all, this method demonstrates the potential of using Brillouin and Raman spectroscopy to attribute mechanical properties to chemical properties.

CHAPTER IV

CONCLUSION

In this report, the proof-of-principle of attributing mechanical properties to biological adipose tissue, skin, and vessel samples of rats was demonstrated. By combining the data from Raman and Brillouin spectroscopy, it was shown that there is indeed an increase in stiffness in adipose tissue when a diet with more lipid is consumed. Implementing a line scan in conjunction with ratios found using Raman spectroscopy was proven to be a potentially worthwhile method of characterizing biological samples. Studies that would be useful in the future to verify and add on to these results include those that compare different storage techniques to the Brillouin shift when transferring biological samples and studies with more rats and samples to analyze. Future work will include using simultaneous Brillouin and Raman spectroscopies to evaluate the drug-induced changes in the elasticity and chemical composition of adipose tissue [36].

REFERENCES

[1] R. S. Ahima, "Adipose Tissue as an Endocrine Organ," *Obes. VO - 14, Suppl. 005*, 2006.

[2] A. Tchernof, C. Bélanger, A.-S. Morisset, C. Richard, J. Mailloux, P. Laberge, and P. Dupont, "Regional differences in adipose tissue metabolism in women: minor effect of obesity and body fat distribution.," *Diabetes*, vol. 55, no. 5, pp. 1353–1360, May 2006.

[3] "Connective tissue supports and protects," *Connexions Website*, 2013. [Online]. Available: http://cnx.org/content/m46049/1.4/ Published .

[4] B. Cannon and J. Nedergaard, "Brown adipose tissue: function and physiological significance.," *Physiol. Rev.*, vol. 84, no. 1, pp. 277–359, Jan. 2004.

[5] V. Catalán, J. Gómez-Ambrosi, A. Rodríguez, and G. Frühbeck, "Role of extracellular matrix remodelling in adipose tissue pathophysiology: relevance in the development of obesity," *Histol. Histopathol.*, vol. 27, no. 12, pp. 1515–1528, 2012.

[6] G. S. Hotamisligil, "Inflammation and metabolic disorders," *Nature*, vol. 444, no. 7121, pp. 860–867, Dec. 2006.

[7] K. Sun, C. C. M. Kusminski, and P. E. P. Scherer, "Adipose tissue remodeling and obesity," *J. Clin. ...*, vol. 121, no. 6, pp. 2094–2101, 2011.

[8] J. K. Sethi and A. J. Vidal-Puig, "Thematic review series: Adipocyte Biology. Adipose tissue function and plasticity orchestrate nutritional adaptation," *J. lipid Res. JLR VO - 48, no. 6*, no. 6, 2007.

[9] N. Alkhouli, J. Mansfield, E. Green, J. Bell, B. Knight, N. Liversedge, J. C. Tham, R. Welbourn, A. C. Shore, K. Kos, and C. P. Winlove, "The mechanical properties of human adipose tissues and their relationships to the structure and composition of the extracellular matrix.," *Am. J. Physiol. Endocrinol. Metab.*, vol. 305, no. 12, pp. E1427–35, 2013.

[10] A. Divoux, J. Tordjman, D. Lacasa, N. Veyrie, D. Hugol, A. Aissat, A. Basdevant, M. Guerre-Millo, C. Poitou, J.-D. Zucker, P. Bedossa, and K. Clement, "Fibrosis in Human

Adipose Tissue: Composition, Distribution, and Link With Lipid Metabolism and Fat Mass Loss.," *Diabetes*, vol. 59, no. 11, pp. 2817–2825, Nov. 2010.

[11] T. Khan, E. S. Muise, P. Iyengar, Z. V Wang, M. Chandalia, N. Abate, B. B. Zhang, P. Bonaldo, S. Chua, and P. E. Scherer, "Metabolic dysregulation and adipose tissue fibrosis: role of collagen VI.," *Mol. Cell. Biol.*, vol. 29, no. 6, pp. 1575–1591, Mar. 2009.

[12] M. Spencer, R. Unal, B. Zhu, P. A. Kern, C. A. Peterson, N. Rasouli, and R. E. McGehee Jr., "Adipose tissue extracellular matrix and vascular abnormalities in obesity and insulin resistance," *J. Clin. Endocrinol. Metab.*, vol. 96, no. 12, pp. E1990–E1998, Dec. 2011.

[13] R. J. Minns, P. D. Soden, and D. S. Jackson, "The role of the fibrous components and ground substance in the mechanical properties of biological tissues: A preliminary investigation," *J. Biomech.*, vol. 6, no. 2, pp. 153–165, Jan. 1973.

[14] E. Ravussin and S. R. Smith, "Increased fat intake, impaired fat oxidation, and failure of fat cell proliferation result in ectopic fat storage, insulin resistance, and type 2 diabetes mellitus," *LIPIDS AND INSULIN RESISTANCE: THE ROLE OF FATTY ACID METABOLISM AND FUEL PARTITIONING*, vol. 967. pp. 363–378, 2002.

[15] L. Casteilla, L. Pénicaud, B. Cousin, and D. Calise, "Choosing an Adipose Tissue Depot for Sampling Factors in Selection and Depot Specificity," vol. 456.

[16] T.-H. Chun, "Peri-adipocyte ECM remodeling in obesity and adipose tissue fibrosis.," *Adipocyte*, vol. 1, no. 2, pp. 89–95, Apr. 2012.

[17] C. Henegar, J. Tordjman, V. Achard, D. Lacasa, I. Cremer, M. Guerre-Millo, C. Poitou, A. Basdevant, J.D. Zucker, K. Clement, V. Stich, N. Viguerie, D. Langin, and P. Bedossa, "Adipose tissue transcriptomic signature highlights the pathological relevance of extracellular matrix in human obesity," *Genome Biol.*, vol. 9, no. 1, Jan. 2008.

[18] A. Gefen and E. Haberman, "Viscoelastic properties of ovine adipose tissue covering the gluteus muscles," *J. Biomech. Eng.*, vol. 129, no. 6, pp. 924–930, Dec. 2007.

[19] C. J. Lyon, R. E. Law, and W. A. Hsueh, "Minireview: Adiposity, inflammation, and atherogenesis," *ENDOCRINOLOGY*, vol. 144, no. 6. pp. 2195–2200.

[20] L. Brillouin, “Diffusion de la lumiere et des rayons X par un corps transparent homogene,” *Ann. Phys.*, vol. 17, pp. 88–122, 1922.

[21] G. D. Hickman, J. M. Harding, M. Carnes, A. Pressman, G. W. Kattawar, and E. S. Fry, “Aircraft laser sensing of sound velocity in water: Brillouin scattering,” *Remote Sens. Environ.*, vol. 36, no. 3, pp. 165–178, Jan. 1991.

[22] E. S. Fry, Y. Emery, X. Quan, and J. W. Katz, “Accuracy limitations on Brillouin lidar measurements of temperature and sound speed in the ocean,” *Appl. Opt.*, vol. 36, no. 27, pp. 6887–6894, Sep. 1997.

[23] K. J. Koski and J. L. Yarger, “Brillouin imaging.,” *Appl. Phys. Lett.*, vol. 87, no. 6, p. 61903, Aug. 2005.

[24] M. H. Manghnani, S. N. Tkachev, P. V Zinin, C. Glorieoux, P. Karvankova, and S. Veprek, “Elastic properties of nc-TiN/a-Si3N4 and nc-TiN/a-BN nanocomposite films by surface Brillouin scattering.,” *J. Appl. Phys.*, vol. 97, no. 5, p. 54308, Mar. 2005.

[25] O. Stachs, S. Reiß, R. Guthoff, and H. Stolz, “Spatially resolved Brillouin spectroscopy for in vivo determination of the biomechanical properties of the crystalline lenses,” in *Progress in Biomedical Optics and Imaging - Proceedings of SPIE*, 2012, vol. 8209, no. Ophthalmic Technologies XXII.

[26] G. Scarcelli and S. H. Yun, “Confocal Brillouin microscopy for three-dimensional mechanical imaging.,” *Nat. Photonics*, vol. 2, no. 1, pp. 39–43, Jan. 2008.

[27] G. Scarcelli, R. Pineda, and S. H. Yun, “Brillouin Optical Microscopy for Corneal Biomechanics,” *INVESTIGATIVE OPHTHALMOLOGY & VISUAL SCIENCE*, vol. 53, no. 1. pp. 185–190.

[28] R. Harley, D. James, A. Miller, and J. W. White, “Phonons and the elastic moduli of collagen and muscle,” *Nature*, vol. 267, no. 5608, pp. 285–287, Jan. 1977.

[29] S. Reiß, G. Burau, H. Stolz, O. Stachs, and R. Guthoff, “Spatially resolved Brillouin spectroscopy to determine the rheological properties of the eye lens,” *Biomed. Opt. Express*, vol. 2, no. 8, pp. 2144–2159, Aug. 2011.

[30] Z. Steelman, Z. Meng, A. J. Traverso, and V. V Yakovlev, "Brillouin spectroscopy as a new method of screening for increased CSF total protein during bacterial meningitis," *J. Biophotonics*, vol. 8, no. 5, pp. 408–414, May 2015.

[31] P. Matousek, I. P. Clark, M. Towrie, A. W. Parker, M. D. Morris, N. Everall, E. Draper, and A. Goodship, "Numerical simulations of subsurface probing in diffusely scattering media using spatially offset Raman spectroscopy," *Appl. Spectrosc.*, vol. 59, no. 12, pp. 1485–1492, Dec. 2005.

[32] Z. K. Meng, A. J. Traverso, and V. V Yakovlev, "Background clean-up in Brillouin microspectroscopy of scattering medium," *OPTICS EXPRESS*, vol. 22, no. 5. pp. 5410–5415.

[33] C. W. Freudiger, W. Min, B. G. Saar, S. Lu, G. R. Holtom, C. He, J. C. Tsai, J. X. Kang, and X. S. Xie, "Label-Free Biomedical Imaging with High Sensitivity by Stimulated Raman Scattering Microscopy," *Sci. VO - 322*, no. 5909, p. 1857, 2008.

[34] Z. Meng and V. V Yakovlev, "Optimizing signal collection efficiency of the VIPA-based Brillouin spectrometer," *J. Innov. Opt. Health Sci.*, vol. 08, no. 04, p. 1550021, Nov. 2014.

[35] A. C. S. Talari, Z. Movasaghi, S. Rehman, and I. ur Rehman, "Raman Spectroscopy of Biological Tissues," *Appl. Spectrosc. Rev.*, vol. 50, no. 1, pp. 46–111, 2015.

[36] M. Troyanova-Wood, C. Gobbell, Z. Meng, and V. V Yakovlev, "Assessing the effect of a high-fat diet on rodents' adipose tissue using Brillouin and Raman spectroscopy," 2016, vol. 9703, pp. 970310–970316.

APPENDIX A

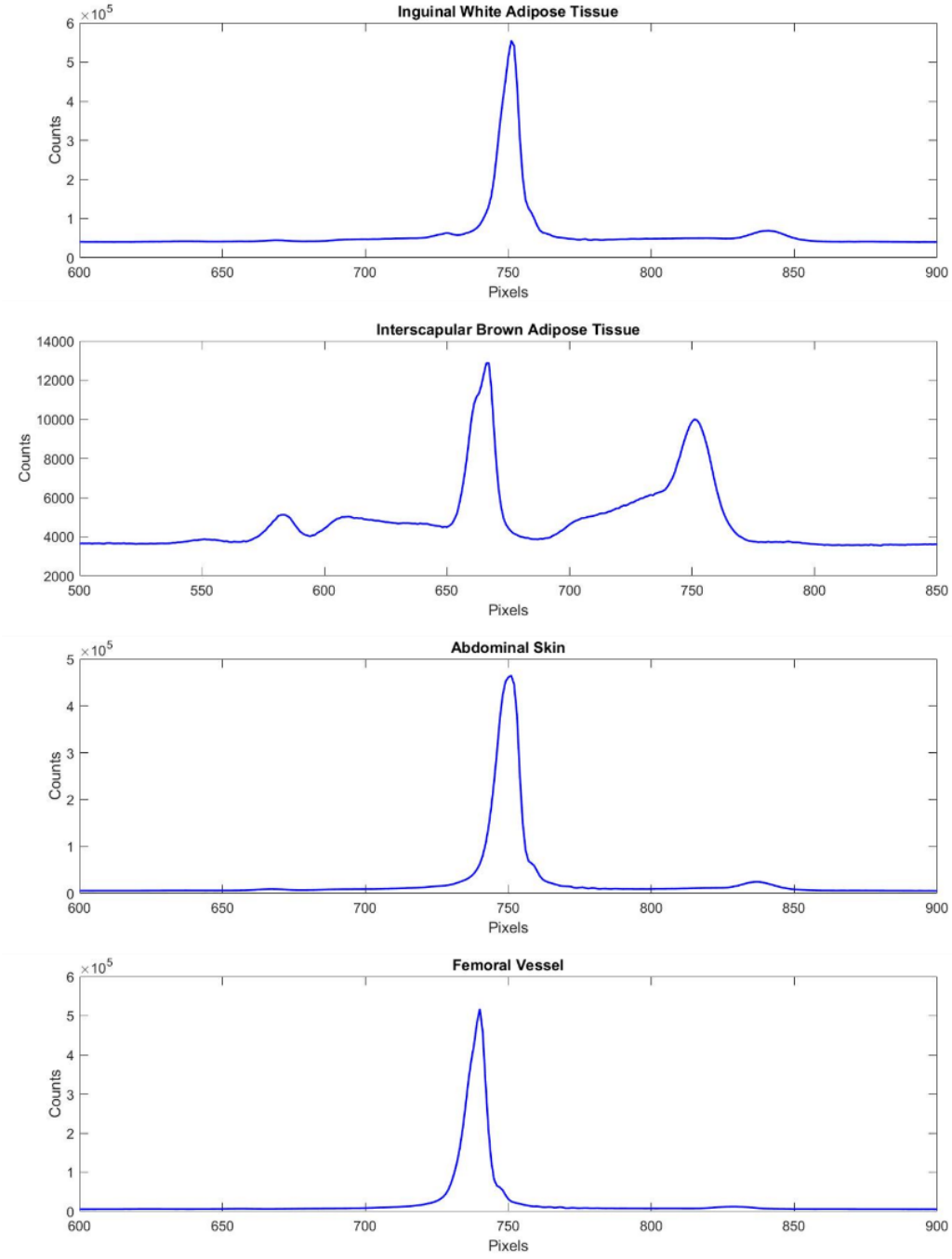

Figure A1. Representative Brillouin spectra for each sample. From top to bottom: Inguinal Adipose Tissue, Interscapular Adipose Tissue, Abdominal Skin, Femoral Vessel. Y-axis units are arbitrary.

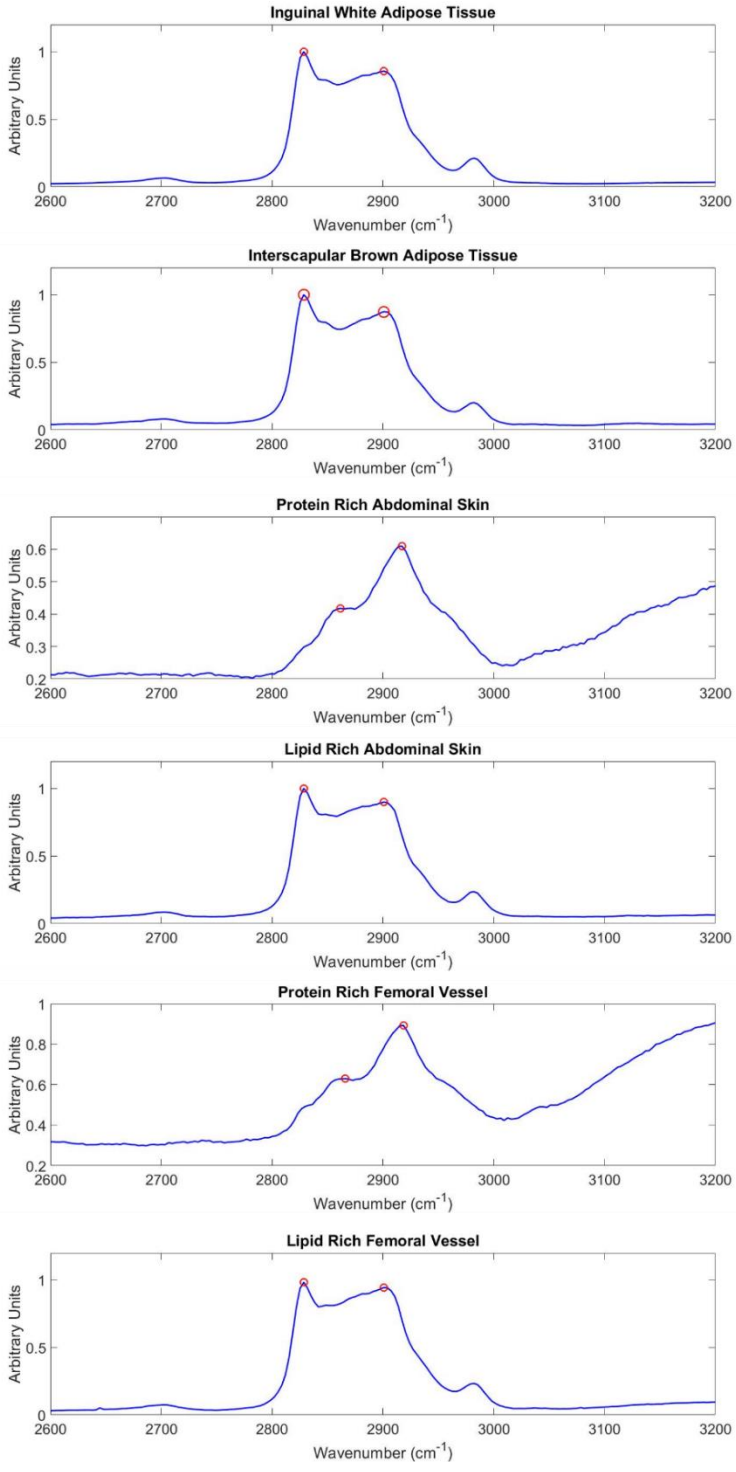

Figure A2. Representative Raman data with each type of sample acquisition. The red dots represent where the peaks were located using MATLAB